International Journal of Electrical and Computer Engineering (IJECE)
Vol. 16, No. 3, June 2026, pp. 1107~1117
ISSN: 2088-8708, DOI: 10.11591/ijece.v16i3.pp1107-1117

Study on the design and comparison of permanent magnet synchronous motors for electric vehicle applications

Pham Ngoc Sam, Tran Duc Chuyen
Faculty of Electrical Engineering – Automation, University of Economics - Technology for Industries, Hanoi, Vietnam

Article Info

Article history:

Received Jan 4, 2026
Revised Mar 27, 2026
Accepted Apr 26, 2026

Keywords:

Analytical model
Electric machine design
Electrical machines
Energy saving
Finite element method
Permanent magnet synchronous motors

ABSTRACT

In this research, the authors present a study analysis and compares two types of embedded internal permanent magnet synchronous motors (IPMSM) with U-type and V-type magnet configurations using finite element method (FEM) modeling to apply these motors to the currently popular electric vehicle industry. Parameters such as magnetic flux density, torque, cogging torque, back electromotive force (back-EMF), torque oscillation, and harmonic components were analyzed and compared; thereby identifying the advantages and disadvantages of the two IPMSM structures. Specifically, the V-type IPMSM motor offers higher efficiency, more stable torque, and a higher quality back electromotive force waveform with lower losses, making it suitable for high-performance applications such as electric vehicles and industrial automation. Meanwhile, the U-type structure has lower cogging torque, suitable for low-speed applications or those requiring high precision. Simulation results from the ANSYS Maxwell software show that the IPMSM motor is energy-efficient, has high power density, and operates smoothly, allowing for rapid acceleration, long range, compact configuration, and low maintenance; it uses permanent magnets on the rotor to eliminate losses, making electric vehicles lighter and more efficient than traditional motors.

Corresponding Author:

Tran Duc Chuyen
Faculty of Electrical Engineering – Automation, University of Economics - Technology for Industries
Hanoi, Vietnam
Email: tdchuyen@uneti.edu.vn

1. INTRODUCTION

Nowadays, the climate change and environmental pollution are pressing global issues, primarily due to the depletion of fossil fuel resources (coal, oil, and natural gas). This is one of the main causes of pollution, especially in urban areas, due to the emission of carbon dioxide (CO_2), nitrogen oxides (NOx), and other pollutants during the combustion of fossil fuels in internal combustion engines. Therefore, electric and hybrid vehicles have become crucial solutions to reduce the environmental impact of transportation. In electric vehicles (EVs), the internal permanent magnet synchronous motor (IPMSM) is the "heart" of the powertrain. The choice of U-shaped or V-shaped rotor structure is not simply a matter of form and size but is also a strategy for current electric vehicle control engineering to optimize performance, torque and high-speed performance during operation [1]–[5].

Among the various types of motors, embedded IPMSM are increasingly popular in electric vehicle and industrial applications due to their high efficiency and high torque [1], [2]. The performance of this type of motor is influenced by many factors, including the magnet configuration [3], [4]. Many studies have focused on optimizing IPMSM and many magnet configurations have been designed and analyzed. In the document [5], V-shaped, double V-shaped and U-shaped magnet configurations were designed for

applications requiring high speed. The results show that the V-shaped magnet configuration has the high performance but lower angular speed due to the high no-load voltage [6]–[9]. The double V-shaped configuration has high losses but a larger angular speed [10]–[12]. The U-shaped configuration has performance between the two types of motors above [13]–[16]. Five permanent magnet (PM) synchronous motor rotor configurations for hybrid buses were designed and compared in the literature [6], including a surface-mounted magnet configuration and four internal-mounted magnet configurations (conventional configuration, fragmented configuration, V-shaped configuration, and double V-shaped configuration) [14], [17]–[22]. The results showed that the PM motor with the fragmented rotor configuration had a wider power-speed constant amplitude than the conventional PM motor. The W-shaped PM motor had high efficiency and a wide speed amplitude. High-quality control is suitable for applications in controlling various types of electric vehicles, resulting in high efficiency and energy savings, this provides high-quality control suitable for application in controlling various types of electric vehicles currently available, aiming to save energy [23]–[26].

As analyzed above, several studies have compared different magnet configurations of IPMSM motors. However, none have focused on the two types of IPM configurations with U-type and V-type magnets. Furthermore, these studies mainly focused on simulating motors using the finite element analysis (FEM) to obtain results. These studies have not yet presented detailed analytical calculations of electromagnetic parameters and have not provided simulation models of the motors. The novelty of this study lies in providing a detailed analytical model to determine the parameters of IPMSM motors with U-type and V-type magnet configurations. Subsequently, the FEM is used to calculate, simulate, and compare the performance of the two IPMSM configurations, such as magnetic flux density, output torque, back electromotive force, and temperature.

2. THE ANALYTICAL STUDY OF DESIGN DATA

This section presents the electrical and magnetic characteristics that influence the sizing and selection of key design parameters. The stator inner diameter (D_{is}) is determined as (1):

$$D_{is} = \sqrt[3]{(4V_r/\pi k_s)} \tag{1}$$

In which, k_s is the shape factor which can be selected in the range of 2 to 3, V_r is the rotor volume determined by the ratio between electromagnetic torque (T) and torque density (TRV), [7]. Then the outer diameter of the rotor (D_{or}) is determined:

$$D_{or} = D_{is} - 2g \tag{2}$$

where g is the length of the air gap (g =1). The cross-sectional area of the air gap (A_g) is determined through the inner diameter of the stator (D_{is}) and the outer diameter of the rotor (D_{or}) using the formula:

$$A_g = \left(\frac{((D_{or}-D_{is})/2)L}{2p}\right).\pi \tag{3}$$

In this formula, L is the machine length, determined by the shape factor (k_s) and the stator inner diameter (D_{is}), and $2p$ is the number of pole pairs. The magnetic flux of the magnet (ϕ_m) is determined as (4):

$$\phi_m = \frac{(B_g.A_g)}{2}.10^{-6} \tag{4}$$

In this formula, B_g is the air gap magnetic flux density (B_g=0.9 is chosen). The magnet length (W_m) is determined as (5):

$$W_m = \frac{\phi_m}{B_m.L} \tag{5}$$

In this formula, B_m is the magnetic flux density of the magnet (B_m=0.87 T). The magnet thickness (d_m) is determined as (6):

$$d_m = \frac{(B_g/\mu_0).g_{eff}}{H_m} \tag{6}$$

In which, g_{eff} is the air gap length ($g_{eff} = g$), μ_0 is the magnetic permeability ($\mu_0 = (4\pi)/10^{-7}$), H_m is the current intensity of the magnet. Based on formula (4), ϕ_m can be calculated:

$$\phi_m = 2\phi_{sy} = 2\phi_{ry} = \frac{Q}{2p}.\phi_t \quad (7)$$

In this formula, ϕ_{sy}, ϕ_{ry}, and ϕ_t are the magnetic fluxes across the stator yoke, rotor yoke, and teeth, respectively. From this, the height of the stator yoke (h_{sy}) and the height of the rotor yoke (h_{ry}) are calculated as (8):

$$h_{sy} = \frac{\phi_m}{2B_{sy}.L.k_i} \text{ and } h_{ry} = \frac{\phi_m}{2B_{ry}.L.k_i} \quad (8)$$

In which, k_i is the compression coefficient (k_i=0.96 is determined in [8], L is the stator length. The cogging width is determined as follows [7], [8]:

$$w_t = \frac{\phi_t}{B_t.L.k_i} \quad (9)$$

The number of turns per coil is determined as (10):

$$N = \frac{U_n}{\sqrt{2}k_w.2\pi f B_g L.10^{-6}.(D_{is})/(2)} \quad (10)$$

In which, U_p is the phase voltage, f is the frequency, q is the number of slots under one phase on one pole, k_w is the concentrated winding coefficient [8]. The small diameter of the groove (b_1) and the large diameter of the groove (b_2) are determined as (11):

$$b_1 = \frac{\pi.(D_{is}+2(h_{so}+h_w))}{Q} - w_t \quad (11)$$

In this formula, h_{so} is the cogging height (h_{so}=1) and h_w is the wedge height (h_w=2).

$$b_2 = \sqrt{4(A_{slot} - A_w).tan(\pi/Q) + b_1^2} \quad (12)$$

where A_{slot} is the slot cross-section, A_w is the wedge cross-section, and Q is the number of slots. The stator slot length (h_s) and stator outer diameter (D_{os}) are determined as (13) and (14):

$$h_s = 2(A_{slot} - A_w)/(b_1 + b_2) \quad (13)$$

$$D_{os} = D_{is} + 2(h_{sy} + h_w + h_s) \quad (14)$$

After the analytical model was developed, a 5.5 kW IPMSM motor with both U-type and V-type magnet configurations was constructed. Table 1 lists the required parameters of the two motors. The authors proceeded to construct and compile the following parameter tables.

Table 1 lists the required parameters for the two motors. Table 2 presents the analytical calculation results of the two IPMSM configurations. The authors will prove these results using the FEM in the following section.

Table 1. The design parameters require IPMSM type V and IPMSM type U

Symbol	Parameter	IPMSM type V	IPMSM type U	Unit
n_N	Rotation speed norm	6000	6000	Rpm
P_{rated}	Rated power	5.5	5.5	kW
U_{rated}	Rated voltage	380	380	V
η	Efficiency	91	91	%
f	Frequency	50	50	Hz
$cos\varphi$	Power factor	0.9	0.9	-
$2p$	The number of poles	10	10	-

Table 2. Main design dimensions of the IPMSM engine

Symbol	Parameter	Value	Unit
D_{os}	Stator outer diameter	219.96	mm
D_{is}	Stator inner diameter	147.12	mm
D_{or}	Rotor outer diameter	145.12	mm
D_{sr}	Rotor shaft diameter	102.52	mm
d_{roto}	Rotor length	147.12	mm
n_r	Stator slot number	12	-
d_{Air}	Air gap length	1	mm
D_{ns}	Magnet thickness	3.7	mm

3. METHODS FOR ANALYZING AND CALCULATING FINITE ELEMENTS

The previous section defined the main dimensions and parameters using an analytical model. This section will present the FEM. In the Euclidean space R3, the set of Maxwell equations is expressed as follows [9], [10]:

$$\nabla \times H = J_s;\ \nabla \times E = -J\omega B;\ \nabla . B = 0 \tag{15}$$

In which, J_s is the current density (A/m2), H is the magnetic field (A/m), E is the electric field (V/m) and B is the magnetic flux density (T). Formula (15) is solved by the constituent laws and boundary conditions in (16) and (17) as follows [10]:

$$B = \mu H, J = \sigma E \tag{16}$$

$$n \times H|_{\Gamma_h} = 0, n.B|_{\Gamma_e} = 0 \tag{17}$$

In which, n is the unit normal vector directed from inside to outside the Ω region (with $\Omega = \Omega_c \cup \Omega_C^c$ J being the current density (A/m2), μ being the permeability, σ being the conductivity (S/m). Field B in (15) is derived from vector A in (18).

$$\mathrm{B} = \nabla \times A \tag{18}$$

Combining (15) and (18), the field E is determined through the scalar potential φ in (19):

$$\mathrm{E} = -\partial_t \mathrm{A} - \nabla . \varphi \tag{19}$$

The electromagnetic field equation written in the Ω domain (IPMSM machine domain) is expressed as [10], [14]–[17]. Based on (15) – (19):

$$\nabla \times \left[\frac{1}{\mu}(\nabla \times A - B)\right] + \sigma\, \partial_t \mathrm{A} = \mathrm{J}_s - \sigma \nabla . \varphi \tag{20}$$

The magnetic flux linkage (ϕ) is defined as follows:

$$\phi = \frac{L}{S}\left(\iint_{\Omega^+} A d\Omega - \iint_{\Omega^-} A d\Omega\right) \tag{21}$$

In which S is the cross-sectional area of the conductor length (L). From there, we have determined the back electromotive force by using the magnetic flux linkage (ϕ) in (21).

4. THE STUDY SIMULATION AND ANALYSIS OF RESULT

Based on the required dimensions from the analytical model in Table 2, the finite element method (FEM) was applied to calculate and simulate the magnetic flux density, torque, cogging torque, back electromotive force, harmonic components, and magnetic flux of the two IPM configurations. Figure 1 and Figure 2 show the 2D models of IPMs with V-shaped and U-shaped magnet configurations. Specifically, Figure 1(a) illustrates the V-type rotor structure, while Figure 1(b) displays its corresponding stator structure. Similarly, Figure 2(a) depicts the U-type rotor structure, and Figure 2(b) shows its respective stator structure. The magnetic flux density distribution of the two IPM configurations is shown in Figures 3. In detail, Figure 3(a) presents the magnetic flux distribution for the V-type magnet IPMSM, whereas Figure 3(b)

demonstrates the distribution for the U-type magnet IPMSM. The maximum magnetic flux density of the V-shaped configuration is 2.399 T, while that of the U-shaped configuration is 2.11 T.

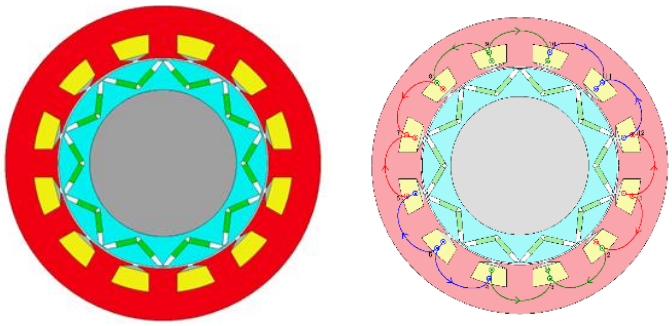

(a) (b)

Figure 1. The model 2D of a V-type magnetic IPMSM (a) V-type rotor structure and (b) V-type stator structure

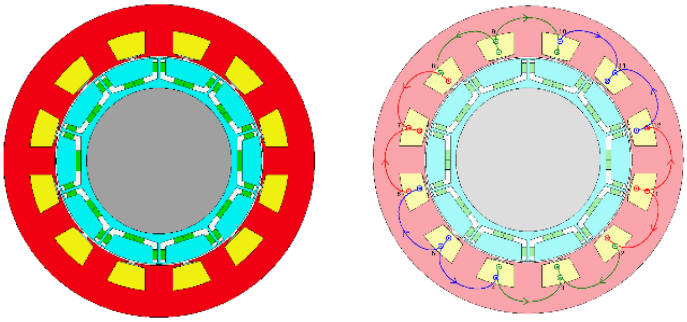

(a) (b)

Figure 2. The model 2D of U-type magnetic IPMPSM (a) U-type rotor structure and (b) U-type stator structure

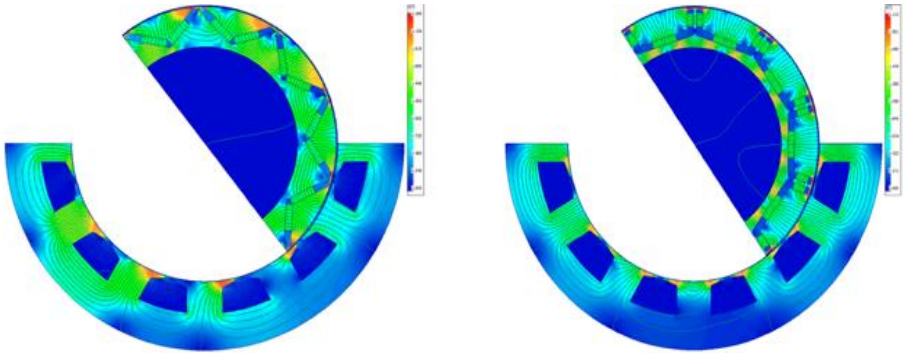

(a) (b)

Figure 3. Magnetic flux distribution of two IPMSP configurations (a) V-type magnet IPMSM and (b) U-type magnet IPMSM motor

The main reason for this is the geometric structure of the magnets and magnetic field lines. The V-shaped magnet directs the two branches of the magnet towards the air gap, creating sharp angles at the pole edges, causing the magnetic field lines to converge strongly at very small points at the rotor pole edges, creating a large maximum magnetic flux, which easily causes local saturation. At the same time, the path of the magnetic flux is short, so the magnetic field distribution is concentrated and less leaky. Conversely, the U-shaped magnet disperses the magnetic field lines over a wider area due to the larger pole angle, thus

resulting in a lower maximum magnetic flux density. However, this distribution makes the magnetic field lines less concentrated and more evenly distributed.

The simulation results in Figure 4 present the torque of the two motor configurations. The average torque value of the V-type IPM configuration is 87.721 Nm, slightly higher than the U-type configuration at 87.658 Nm. However, the oscillation characteristics of the two configurations differ. In the V-type configuration, the torque is stable and oscillates less, depends on the concentrated magnetic flux distribution in the air gap. This reduces the variation with the rotor position, resulting in smoother torque. Conversely, in the U-type configuration, the torque exhibits more pronounced oscillations. This is due to the magnetic flux distribution and leakage branches inside the rotor, causing the torque to be affected by flux ripples. Figure 5 shows the cogging torque of the two IPM configurations. The simulation results show a clear difference between the two configurations. In V-type IPMs, the torque range is quite large, fluctuating between -2.8 Nm and 2 Nm, compared to U-types which range from -1.3 to 1.6 Nm. This means that U-types operate more smoothly at low speeds. The main reason is that the V-shaped magnet structure creates localized areas of magnetic concentration at the pole edges, causing the magnetic attraction force to change significantly when interacting with the stator teeth.

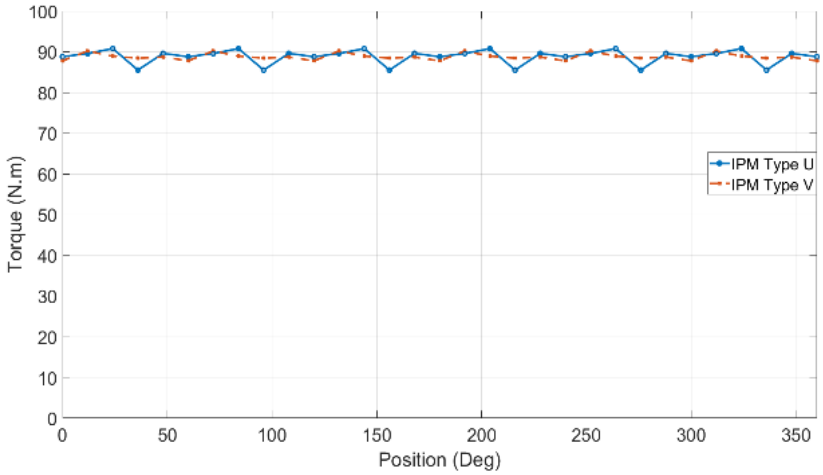

Figure 4. Torque of U-type and V-type magnetic IPM

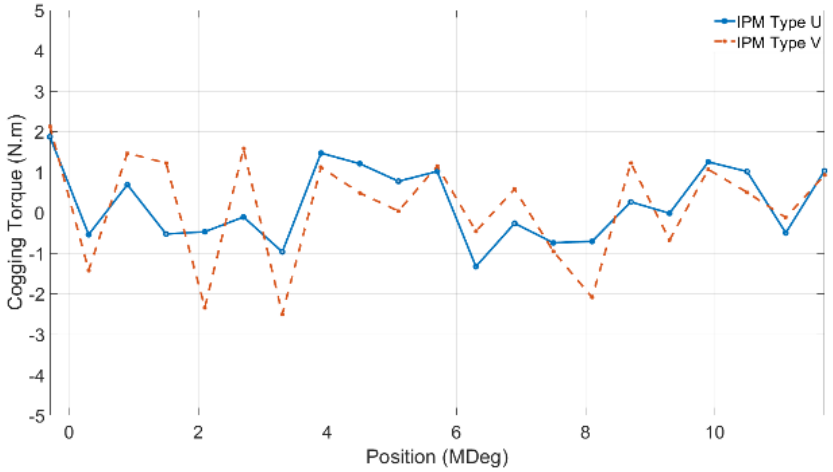

Figure 5. IPM cogging torque of U-type and V-type magnets

Figure 6 illustrates the back electromotive force of U-type and V-type IPMs. The results show that both IPM configurations produce near-sinusoidal waveforms, although there are slight differences. The peak amplitude of the V-type is slightly higher than that of the U-type, indicating better flux utilization.

Furthermore, the waveform of the V-type magnet is more uniform and less distorted, while the U-type exhibits slight distortion at extreme points. This means that the V-type IPM has higher quality back electromotive force, helping the motor achieve better electromechanical conversion efficiency and limiting losses due to voltage waveform distortion. Figure 7 shows that the harmonic spectra of both IPM configurations have a dominant fundamental component. However, the V-type IPM exhibits lower-order harmonics (especially the 5th and 7th orders) with larger amplitudes compared to the U-type. Conversely, in the U-type, higher-order harmonics (such as the 11th and 13th orders) are slightly more prominent. This indicates that the V-type IPM still exhibits distortion at low harmonics, while the U-type configuration tends to have distortion at high harmonics.

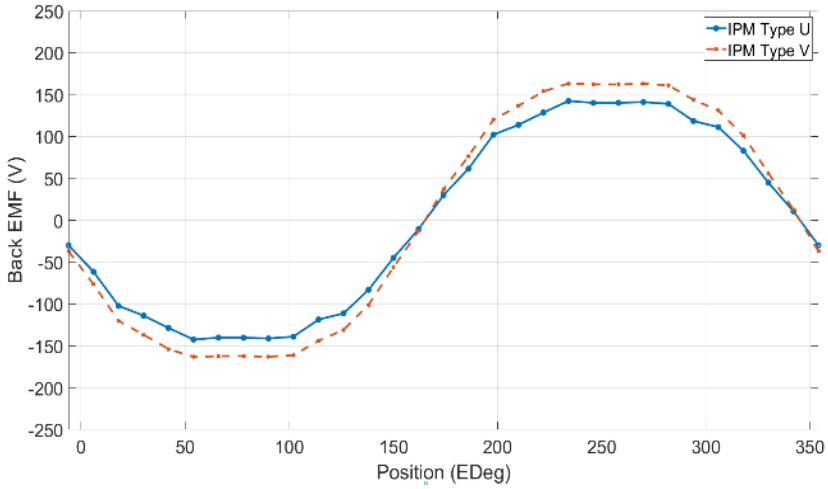

Figure 6. Back electromotive force (EMF) of U-type and V-type magnetic IPM

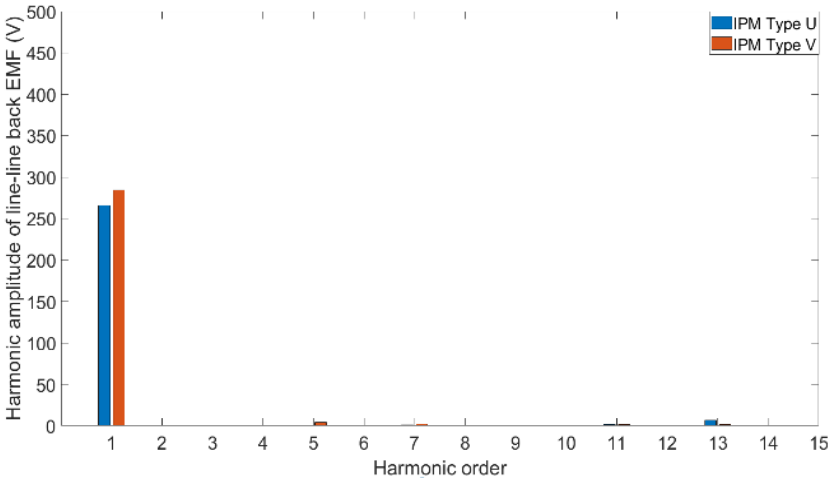

Figure 7. Harmonic waves of U-type and V-type magnet IPM

Figure 8 shows the torque oscillation of the two motor configurations. The V-type IPM has a narrower oscillation range, from -1.3 Nm to 1.6 Nm, while the U-type has a wider oscillation range, from -4 to 2.2 Nm. This indicates that the V-type magnet configuration is more optimal in terms of torque oscillation, suitable for applications requiring consistent torque with minimal vibration, while the U-type configuration may cause vibration and noise when the load changes. Figure 9 shows the flux linkage of the two motors. Both the U-type and V-type magnet configurations produce near-sinusoidal waveforms, but the maximum amplitude of the U-type is slightly larger, demonstrating stronger flux linkage with the stator windings.

The performance characteristics of V- and U-shaped magnet configuration IPMs are presented in Table 3. The V-type IPM motor has an efficiency of 93.567%, higher than the U-type IPM with a value of 91.887%. The total losses of the V-type IPM are 378.94 W, significantly lower than the U-type configuration's 482.26 W. This difference is mainly due to the more concentrated magnetic flux distribution in the V-type magnet configuration, which allows for better utilization of magnetic field energy. Conversely, in the U-type, the magnetic flux is more evenly distributed but has more leakage and distorted harmonics, leading to greater losses and lower efficiency.

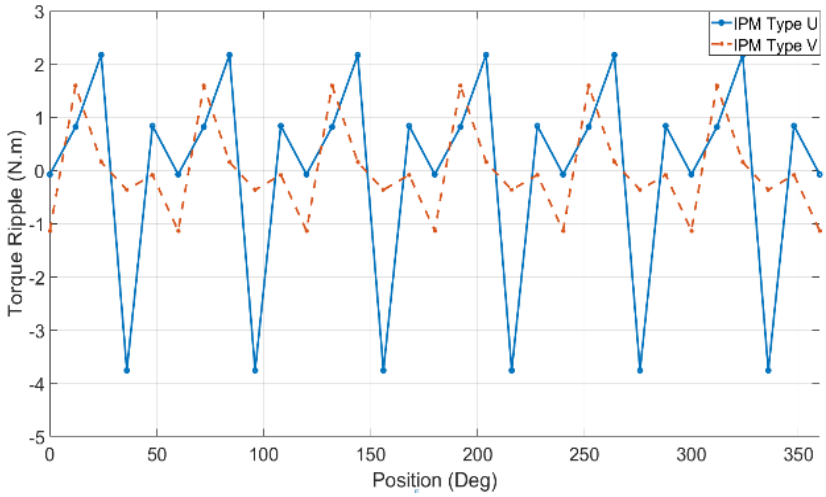

Figure 8. Torque oscillations of U-type and V-type magnetic IPM

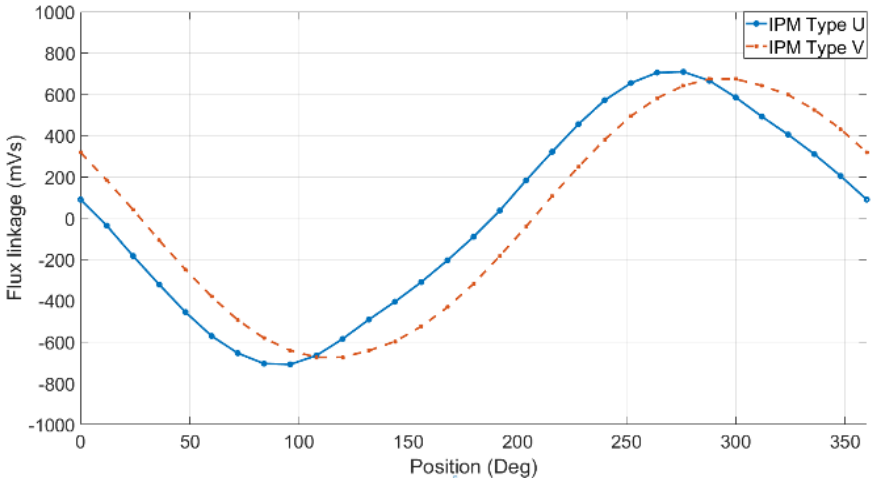

Figure 9. Magnetic flux linkage of U-type and V-type magnet IPM

Table 3. Results of the finite element analysis method

Symbol	Simulation results	IPMSM type V	IPMSM type U	Unit
η	Efficiency	93.567	91.887	%
τ	Torque	87.721	87.658	Nm
τ_d	Disturbance moment	2.4236	5.8529	%
$cos\varphi$	Power factor	0.89179	0.80266	-
P_{out}	Output Power	5511.7	5507.7	W
P_{tt}	Total Losses (on load)	378.94	486.26	W

5. CONCLUSION

This study combines analytical modeling and finite element methods to investigate IPM motors with U-type and V-type magnet configurations. Characteristic electromagnetic parameters such as magnetic flux density, torque, back electromotive force, cogging torque, torque oscillation, flux linkage, and harmonic components were analyzed in detail. The results show that both magnet configurations have their own advantages and disadvantages. Specifically, the V-type magnet IPM exhibits higher efficiency, lower total losses, and smaller torque oscillations. Furthermore, the back electromotive force waveform of this configuration is smoother and less distorted, contributing to increased operational stability, making it suitable for applications requiring high performance and stability such as electric vehicle drive systems, industrial robots, heavy-duty industrial equipment requiring continuous operation, compressors, and high-speed pumps. On the other hand, U-type IPMs have lower cogging torque and larger flux linkage amplitude, which is advantageous in some applications requiring smoothness at low speeds, such as medical devices and smart home appliances. Overall, the optimal configuration selection still depends on the specific requirements of each application, especially in the current electric vehicle sector. Furthermore, the results obtained from the finite element simulation in this study can serve as a reference for selecting suitable IPM magnet configurations in practical designs. This research can be expanded and further developed by combining it with modern optimization methods such as swarm algorithms and genetic algorithms to improve design performance.

ACKNOWLEDGEMENTS

This research was supported by Faculty of Electrical Engineering-Automation, University of Economics - Technology for Industries, Vietnam.

FUNDING INFORMATION

Authors state no funding involved.

AUTHOR CONTRIBUTIONS STATEMENT

This journal uses the Contributor Roles Taxonomy (CRediT) to recognize individual author contributions, reduce authorship disputes, and facilitate collaboration.

AUTHOR CONTRIBUTIONS STATEMENT

This journal uses the Contributor Roles Taxonomy (CRediT) to recognize individual author contributions, reduce authorship disputes, and facilitate collaboration.

Name of Author	C	M	So	Va	Fo	I	R	D	O	E	Vi	Su	P	Fu
Pham Ngoc Sam	✓	✓	✓	✓	✓	✓	✓	✓	✓	✓	✓		✓	✓
Tran Duc Chuyen	✓	✓	✓	✓	✓	✓	✓		✓	✓	✓	✓	✓	✓

C : **C**onceptualization
M : **M**ethodology
So : **So**ftware
Va : **Va**lidation
Fo : **Fo**rmal analysis
I : **I**nvestigation
R : **R**esources
D : **D**ata Curation
O : Writing - **O**riginal Draft
E : Writing - Review & **E**diting
Vi : **Vi**sualization
Su : **Su**pervision
P : **P**roject administration
Fu : **Fu**nding acquisition

CONFLICT OF INTEREST STATEMENT

Authors state no conflict of interest.

INFORMED CONSENT

We have obtained informed consent from all individuals included in this study.

ETHICAL APPROVAL

The research related to human use has been complied with all the relevant national regulations and institutional policies in accordance with the tenets of the Helsinki Declaration and has been approved by the authors' institutional review board or equivalent committee.

DATA AVAILABILITY

Data availability is not applicable to this paper as no new data were created or analyzed in this study.

REFERENCES

[1] A. Sharma and B. N. Phadke, "Advantages of IPM motor in electrical propulsion over other motors for electrical vehicles," *International Journal of Scientific Progress and Research (IJSPR)*, vol. 14, no. 01, pp. 1–3, 2015.

[2] J. Wu, J. Wang, C. Gan, Q. Sun, and W. Kong, "Efficiency optimization of PMSM drives using field-circuit coupled FEM for EV/HEV applications," *IEEE Access*, vol. 6, pp. 15192–15201, 2018, doi: 10.1109/ACCESS.2018.2813987.

[3] S. Wu, L. Tian, and S. Cui, "A comparative study of the interior permanent magnet electrical machine's rotor configurations for a single shaft hybrid electric bus," in *2008 IEEE Vehicle Power and Propulsion Conference, VPPC 2008*, 2008. doi: 10.1109/VPPC.2008.4677789.

[4] H. Chen and C. H. T. Lee, "Parametric sensitivity analysis and design optimization of an interior permanent magnet synchronous motor," *IEEE Access*, vol. 7, pp. 159918–159929, 2019, doi: 10.1109/ACCESS.2019.2950773.

[5] T. Husain and S. T. Lee, "Design considerations for magnet configurations in IPM rotor for high speed traction applications," in *2019 IEEE Energy Conversion Congress and Exposition, ECCE 2019*, 2019, pp. 6062–6069. doi: 10.1109/ECCE.2019.8912958.

[6] A. Wang, Y. Jia, and W. L. Soong, "Comparison of five topologies for an interior permanent-magnet machine for a hybrid electric vehicle," *IEEE Transactions on Magnetics*, vol. 47, no. 10, pp. 3606–3609, 2011, doi: 10.1109/TMAG.2011.2157097.

[7] M. Ojaghi, M. Sabouria, J. Faizb, and V. Ghorbanianb, "Exact modeling and simulation of saturated induction motors with broken rotor bars fault using winding function approach," *International Journal of Engineering, Transactions A: Basics*, vol. 27, no. 1, pp. 69–78, 2014, doi: 10.5829/idosi.ije.2014.27.01a.10.

[8] P. Roy, "Thermal modeling of permanent magnet synchronous motors for electric vehicle application," Master Thesis, University of Windsor, 2020.

[9] J. Y. Choi, H. Il Park, S. M. Jang, and S. H. Lee, "Design and analysis of surface-mounted PM motor of compressor for electric vehicles applications according to slot/pole combinations," *Transactions of the Korean Institute of Electrical Engineers*, vol. 60, no. 10, pp. 1846–1857, Oct. 2011, doi: 10.5370/KIEE.2011.60.10.1846.

[10] Z. Q. Zhu and D. Howe, "Influence of design parameters on cogging torque in permanent magnet machines," *IEEE Transactions on Energy Conversion*, vol. 15, no. 4, pp. 407–412, 2000, doi: 10.1109/60.900501.

[11] J. Wang, W. Geng, J. Guo, L. Li, and Z. Zhang, "Design and performance comparison of novel flux-concentrating IPM machines for power generation system application of extended-range electric vehicle," *IEEE Transactions on Industrial Electronics*, vol. 70, no. 5, pp. 4450–4460, May 2023, doi: 10.1109/TIE.2022.3183341.

[12] S. A. Khalil, M. Yousif, F. Khan, and U. Jadoon, "Design and analysis of spoke-type inverted V shape IPMSM with concentrated winding for EV applications," in *2025 International Conference on Emerging Power Technologies, ICEPT 2025*, Apr. 2025, pp. 1–6. doi: 10.1109/ICEPT66058.2025.11036224.

[13] Y. Yang *et al.*, "Design and comparison of interior permanent magnet motor topologies for traction applications," *IEEE Transactions on Transportation Electrification*, vol. 3, no. 1, pp. 86–97, 2017, doi: 10.1109/TTE.2016.2614972.

[14] Q. Chen, J. Liao, Z. Sang, W. Qian, G. Xu, and Z. Liu, "Design and analysis of a novel hybrid rotor PM machine considering negative torque ripple contribution," *IEEE Transactions on Industrial Electronics*, vol. 71, no. 7, pp. 6775–6786, Aug. 2024, doi: 10.1109/TIE.2023.3299034.

[15] Y. Yang, N. Schofield, and A. Emadi, "Integrated electromechanical double-rotor compound hybrid transmissions for hybrid electric vehicles," *IEEE Transactions on Vehicular Technology*, vol. 65, no. 6, pp. 4687–4699, 2016, doi: 10.1109/TVT.2015.2487301.

[16] M. A. Muqsit, U. Habib, U. Ur Rehman, and M. Irfan, "Design and validation of an analytical framework for BLDC motors," in *2025 International Conference on Emerging Power Technologies, ICEPT 2025*, Apr. 2025, pp. 1–6, doi: 10.1109/ICEPT66058.2025.11036196.

[17] P. H. Nam and T. Đ. Chuyen, "The BLDC motor design for current industrial and civil applications," *Journal Européen des Systèmes Automatisés*, vol. 58, no. 11, pp. 2427–2433, Nov. 2025, doi: 10.18280/jesa.581119.

[18] M. S. Rafaq, W. Midgley, and T. Steffen, "A review of the state of the art of torque ripple minimization techniques for permanent magnet synchronous motors," *IEEE Transactions on Industrial Informatics*, vol. 20, no. 1, pp. 1019–1031, Jan. 2024, doi: 10.1109/TII.2023.3272689.

[19] P. H. Nam and T. D. Chuyen, "Research on optimal design of surface permanent magnet synchronous generator," *Bulletin of Electrical Engineering and Informatics*, vol. 14, no. 5, pp. 4115–4124, Oct. 2025, doi: 10.11591/eei.v14i5.10305.

[20] X. Liu, H. Chen, J. Zhao, and A. Belahcen, "Research on the performances and parameters of interior PMSM used for electric vehicles," *IEEE Transactions on Industrial Electronics*, vol. 63, no. 6, pp. 3533–3545, 2016, doi: 10.1109/TIE.2016.2524415.

[21] Y. Xiao, Z. Q. Zhu, G. W. Jewell, J. T. Chen, D. Wu, and L. M. Gong, "Influence of armature reaction on magnetic-field-shift effect in asymmetric interior permanent magnet machines," *IEEE Transactions on Energy Conversion*, vol. 37, no. 2, pp. 1475–1488, Jun. 2022, doi: 10.1109/TEC.2021.3132588.

[22] Y. Yang, K. A. Ali, J. Roeleveld, and A. Emadi, "State-of-the-art electrified powertrains - hybrid, plug-in, and electric vehicles," *International Journal of Powertrains*, vol. 5, no. 1, p. 1, 2016, doi: 10.1504/ijpt.2016.075181.

[23] A. Ghaedi and H. Gorginpour, "Reliability evaluation of permanent magnet synchronous generator-based wind turbines considering wind speed variations," *Wind Energy*, vol. 24, no. 11, pp. 1275–1293, Nov. 2021, doi: 10.1002/we.2631.

[24] F. Wang, Y. Zhu, H. Wang, and D. Zhao, "Design and Analysis of a Bearingless Permanent-Magnet Motor for Axial Blood Pump Applications," *IEEE Access*, vol. 8, pp. 7622–7627, 2020, doi: 10.1109/ACCESS.2019.2959633.

[25] Y. Meng, S. Fang, Z. Pan, W. Liu, and L. Qin, "Design and analysis of a new partitioned stator hybrid-excited flux reversal machine with dual-PM," *IEEE Transactions on Magnetics*, vol. 58, no. 2, pp. 1–6, Feb. 2022, doi: 10.1109/TMAG.2021.3077035.

[26] A. Lakhdara, T. Bahi, Y. Izgheche, and A. Henchiri, "Improving speed tracking performance of PMSM-driven electric vehicles using a hybrid SMCMPC approach," *Journal Europeen des Systemes Automatises*, vol. 58, no. 9, pp. 1823–1829, 2025, doi: 10.18280/jesa.580905.

BIOGRAPHIES OF AUTHORS

Pham Ngoc Sam received the degree of automation engineer from Ho Chi Minh City University of Technology and Education, Vietnam, in 1999, and a master's degree in automation from Vietnam Academy of Agriculture in 2012. He is currently a lecturer and a member of the Department of Industrial Electrical, Faculty of Electrical Engineering, University of Economics-Technology for Industries. His research areas include motion control, electric machine design, electrical machines, control systems and their applications, electrical machine control, and industrial automation. He can be contacted at email: pnsam@uneti.edu.vn.

Tran Duc Chuyen received the Ph.D. degree in industrial automation from Le Qui Don Technical University (MTA), Hanoi, Vietnam, in 2016, and became an associate professor in 2024. He currently works at the Faculty of Electrical - Automation, University of Economics-Technology for Industries. He is also the president of the science council of the Faculty of Electrical - Automation. Assist. Prof. Tran Duc Chuyen's main research areas include electric machine design, electrical machines, drive systems, automatic control theory, power electronics and applications, adaptive control, neural network control, robotic control, motion control, microcontrollers and IoT, intelligent control, and artificial intelligence. He can be contacted at email: tdchuyen@uneti.edu.vn.